Research Article | Vol. 28, No. 7 / 30 March 2020 / Optics Express 9340

Optics EXPRESS

Sub-nanometer height sensitivity by phase shifting interference microscopy under environmental fluctuations

AZEEM AHMAD,[1,3] VISHESH DUBEY,[1] ANKIT BUTOLA,[2] JEAN-CLAUDE TINGUELY,[1] BALPREET SINGH AHLUWALIA,[1,4] AND DALIP SINGH MEHTA[2]

[1]*Department of Physics and Technology, UiT The Arctic University of Norway, Tromsø 9037, Norway*
[2]*Department of Physics, Indian Institute of Technology Delhi, Hauz Khas, New Delhi 110016, India*
[3]*ahmadazeem870@gmail.com*
[4]*balpreet.singh.ahluwalia@uit.no*

Abstract: Phase shifting interferometric (PSI) techniques are among the most sensitive phase measurement methods. Owing to its high sensitivity, any minute phase change caused due to environmental instability results into, inaccurate phase measurement. Consequently, a well calibrated piezo electric transducer (PZT) and highly-stable environment is mandatory for measuring accurate phase map using PSI implementation. Here, we present an inverse approach, which can retrieve phase maps of the samples with negligible errors under environmental fluctuations. The method is implemented by recording a video of continuous temporally phase shifted interferograms and phase shifts were calculated between all the data frames using Fourier transform algorithm with a high accuracy $\leq 5.5 \times 10^{-4}\ \pi$ rad. To demonstrate the robustness of the proposed method, a manual translation of the stage was employed to introduce continuous temporal phase shift between data frames. The developed algorithm is first verified by performing quantitative phase imaging of optical waveguide and red blood cells using uncalibrated PZT under the influence of vibrations/air turbulence and compared with the well calibrated PZT results. Furthermore, we demonstrated the potential of the proposed approach by acquiring the quantitative phase imaging of an optical waveguide with a rib height of only 2 nm and liver sinusoidal endothelial cells (LSECs). By using 12-bit CMOS camera the height of shallow rib waveguide is measured with a height sensitivity of 4 Å without using PZT and in presence of environmental fluctuations.

1. Introduction

Digital holographic microscopy (DHM) is a quantitative phase imaging (QPI) technique that has the capability to record the complex wavefront (amplitude as well as phase) of the light field interrogated with the specimen [1–3]. In digital interference microscopy, the complex information about the specimen is encoded in the form of spatially modulated signal generated due to its coherent superposition with the reference field and eventually captured by the area detector, i.e., charge coupled device (CCD)/complementary metal oxide semiconductor (CMOS). The encoded information can be further recovered by employing either single-shot or multi-shot phase retrieval algorithms [4,5] depending upon the recording geometries broadly classified as an off-axis and an on-axis interferometric configurations [6–8].

An off-axis digital interference microscopy can recover information related to specimen from a single interferogram, which makes it suitable to study dynamical behavior of biological cells or tissues [3,6,8]. However, it utilizes maximum one-fourth of the detector's bandwidth for the noise (DC and twin image) free phase recovery. As a consequence, resolution of the reconstructed object field is limited irrespective of the detector's capability, which records

#384259 https://doi.org/10.1364/OE.384259
Journal © 2020 Received 26 Nov 2019; revised 27 Jan 2020; accepted 27 Jan 2020; published 18 Mar 2020

Optics EXPRESS

diffraction limited information about the specimen. To overcome this limitation, on-axis digital interference microscopy attracted strong attention of many researchers, which can utilize full resolving power of CCD/CMOS cameras [9]. Nevertheless, it needs multiple phase shifted interferograms for noise (DC and twin image) free phase recovery of biological specimens at full detector resolution [9].

To date, a significant amount of work has been done in the development of various phase shifting interferometry (PSI) techniques [10]. PSI techniques have been most commonly used for various applications in optical metrology, digital holography and quantitative phase microscopy [1,7,11]. However, most of the PSI techniques utilize expensive piezo electric transducer (PZT) to introduce equal amount of phase shift (δ) between sequentially recorded interferograms [7,11–13]. Further, PSI is extremely sensitive to rapid and imprecise movement of PZT and environmental instability because fringe formation results from the path differences of the order of wavelength of light. Even a small amount of error in PZT calibration, which occurs due to the backlash and hysteresis, can lead to the nonlinear phase shift between data frames resulting in phase measurement errors, such as background modulation errors in the reconstructed phase maps of the target, see results of Refs. [5,14–21]. The background modulation errors have been minimized previously by employing various generalized phase shifting algorithms given in Refs. [5,21–25]. However, with these algorithms, the modulated phase error has not been completely removed in the reconstructed phase maps. In addition, these algorithms are implemented for the phase recovery of either simulated or industrial objects such as low roughness gauge block and resolution chart.

Many asynchronous demodulation methods [26–28] and self-detuning algorithms [29,30] have also been proposed in the past to overcome these modulation errors from the reconstructed phase maps. In addition, two-step demodulation methods [31,32] have been proposed for the phase recovery, which do not reconstruct the phase with good accuracy. The performances of these algorithms are tested either theoretically on the simulated objects or on experimentally recorded interferograms generated due to the superposition of two coherent beams. Further, PSI based on such algorithms would also require expensive phase shifting devices like PZT, spatial light modulators, digital micro mirror devices etc. and sophisticated electronic control systems to introduce phase shift between data frames. In addition, these algorithms in terms of phase sensitivity have not been tested on the objects which introduce small phase shifts such as small optical thickness of sub-10 nm.

Further, various single-shot or simultaneous PSI techniques have also been developed in the past [33–36]. These techniques require either four CCD camera with complex experimental setup or single CCD camera having a micro-polarizer array to record four phase shifted interferograms simultaneously. This either increases cost of the system significantly or leads to inefficient utilization of CCD chip as each four phase shifted interferogram uses only one fourth pixels of the CCD chip [33,34]. All these aforementioned issues related to PSI compel us to think about a straightforward and cost effective method which can avoid the use of expensive phase shifting devices, large number of the optical components and most importantly alleviate the problem of external air turbulence and vibrations.

In this paper, we propose a novel approach that is capable to retrieve accurate phase information of the specimen with high precision without the need of PZT calibrated phase shifted frames. The method is implemented with the recording of a time lapsed interferometric movie of the specimens in presence of external vibration/air turbulence. Subsequently, accurate measurement of the phase shift between the individual interferometric frames of the recorded movie is done using the proposed algorithm. This eradicates the use of any expensive phase shifting devices for the implementation of PSI techniques to perform phase/height measurements of the specimens. The method can even utilize external air turbulence/vibrations to introduce phase shift between frames to determine the phase maps related to specimens. Various unconventional methods such

Optics EXPRESS

as cell phone vibration, artificial air turbulence generated from hair dryer, and manual translation of reference or sample arm was utilized to introduce temporal phase shift in the data frames and consequently utilized for successful phase reconstruction.

The present approach is tested on a standard optical strip waveguide structure and compared with the results obtained from PZT assisted PSI. The proposed approach is further implemented for the phase measurement of the light field interacted with human red blood cells (RBCs), shallow rib waveguide structures (2–8 nm) and liver sinusoidal endothelial cells (LSECs) (H ~ 100 nm). The present approach provides accurate quantitative phase measurement of 2–8 nm rib waveguides with height measurement sensitivity of < 4 Å. Another, advantage of the proposed approach is that it can be implemented for any number of step, for example, 3-step, 4-step,. . . . . , N-step PSI depending upon the speed of recording device. This is advantageous as the phase measurement accuracy increases with the increase in phase steps [14,37]. In the present study, we will discuss advantages, results and opportunities associated with our present method.

2. The proposed method: Theory and simulations

First, the influence of two important parameters phase shift error (α_t) during recording of phase shifted interferograms and utilization of wrong phase shift value (δ) during reconstruction on the phase measurements of specimens is studied both through simulations and experiments. It is observed that precise knowledge of these two parameters is mandatory for the accurate assessment of phase maps using phase shifting based DHM/QPI techniques.

2.1. Five frame phase shifting algorithm

The five frame phase shifting algorithm is widely preferred over the other phase shifting interferometry because of moderate phase error and acquisition time [5]. There is a trade-off between phase shift error and acquisition time, i.e., if one tries to decrease the phase shift error by increasing the number of frames (say N), the acquisition time gets increased or vice versa. However, phase shift error cannot be completely removed even for N-step phase shifting algorithm because of the environmental instability. Hariharan [5] proposed a five frame phase shifting algorithm for the phase measurement with acceptable phase measurement error. The intensity modulation of five phase shifted 2D interferograms at a particular wavelength recorded by WL-PSIM can be expressed as follows [5]:

$$I_1(x,y) = A(x,y) + B(x,y) + 2\sqrt{A(x,y)B(x,y)}\cos[\phi(x,y) - 2\delta + \alpha_t] \tag{1}$$

$$I_2(x,y) = A(x,y) + B(x,y) + 2\sqrt{A(x,y)B(x,y)}\cos[\phi(x,y) - \delta] \tag{2}$$

$$I_3(x,y) = A(x,y) + B(x,y) + 2\sqrt{A(x,y)B(x,y)}\cos[\phi(x,y)] \tag{3}$$

$$I_4(x,y) = A(x,y) + B(x,y) + 2\sqrt{A(x,y)B(x,y)}\cos[\phi(x,y) + \delta] \tag{4}$$

$$I_5(x,y) = A(x,y) + B(x,y) + 2\sqrt{A(x,y)B(x,y)}\cos[\phi(x,y) + 2\delta] \tag{5}$$

where, A(x, y). and B(x, y) are the intensities of two light beams. ϕ(x, y) is the phase information related to test object, δ is the phase shift between two consecutive phase shifted frames and α_t corresponds to the time varying phase shift error between data frames due to external vibrations. The phase information 'ϕ(x, y)' related to test object can be calculated from the following expression if $\alpha_t = 0$[5]:

$$\phi(x,y) = \tan^{-1}\left[\sin\delta\frac{2(I_4(x,y) - I_2(x,y))}{I_1(x,y) - 2I_3(x,y) + I_5(x,y)}\right] \tag{6}$$

The phase map can be further utilized to calculate corresponding height map 'H(x, y)' using the following relation:

Optics EXPRESS

$$H(x,y) = \frac{\lambda}{4\pi(n_s(x,y) - n_m(x,y))}\phi(x,y) \tag{7}$$

where, λ is the central wavelength of light source, $n_s(x, y)$ is the refractive index of sample and $n_m(x, y)$ is the refractive index of surrounding medium. The refractive index of the sample is involved in the calculation of height map in Eq. (7). The samples used throughout the work, are transparent in nature like an optical waveguide fabricated on a reflecting Si-wafer and the biological cells prepared on a reflecting surface. Thus, the light is passed through the sample as well and its refractive index is involved in the calculation.

A simulation study is done to understand the effect of both the phase shift 'δ' between two frames (as described in Eq. (6)) and the time varying phase shift error 'α_t' between the frames (as described in Eq. (1)) on the quantitative phase measurement that occurs during the recording of phase shifted interferograms. Phase shifting interferometry (PSI) or holography techniques are very sensitive to external vibrations or air turbulence, which makes them challenging to implement for accurate quantitative imaging of specimen. In addition, an uncalibrated phase shifter can introduce an unwanted error in the phase measurement. The collective effect of errors of the phase measurement is simulated and studied for five frame phase shifting algorithm [5].

2.2. Simulations

2.2.1. Influence of 'α_t' and 'δ' on the phase measurement

First, the effect of 'α_t,' on the phase measurement during the reconstruction step using Eq. (1) is studied. Five equal phase shifted interferograms are simulated, four of them having equal phase shift ~ 70° and the other one having different phase shifts (determined by α_t). These five phase shifted frames are utilized to retrieve phase map using Eq. (6). To understand the effect of 'α_t', a range of values from – 20° to 20° at an interval of 5° are used in Eq. (1). Note $\alpha_t = 0°$ corresponds to no phase shift error. The value of 'δ' equal to 70° is used into Eq. (6) during reconstruction. It is observed from the simulation results that phase shift error 'α_t' leads to the generation of modulated background noise in the reconstructed phase maps (see Fig. 1(a)). In addition, it is observed that the frequency of the modulated background noise is twice than that of the interferograms spatial frequency. This exhibits a good agreement with the previous studies [5]. The reconstructed phase maps corresponding to each value of phase shift error are shown in Fig. 1(a). Importantly, it can be clearly visualized from the phase images that peak to valley (PV) phase error gets prominent as the value of 'α_t' is deviated from true phase shift.

Figure 1(b) depicts the line profiles of the reconstructed phase maps corresponding to a range of phase shift error 'α_t' used in the Eq. (1). Note that background modulation follows the symmetric trend as 'α_t' go away from 0° towards lower and upper side. Figure 1(c) illustrates the plot of maximum PV error as a function of 'α_t'. The peak to valley phase error is found to be equal to 200 mrad for α_t = - 20° and 20°, whereas, zero exactly at $\alpha_t = 0°$. Therefore, in order to overcome such type of severe issues from the phase images, phase shift error must be equal to zero during the recording of all phase shifted interferograms. This situation is analogous to the nonlinear drift of the phase shifter, which could arises due to the hysteresis and thermal drift of PZT [5]. In addition, air turbulence or vibration could also affect the measurement and introduce unwanted phase shift error 'α_t' between the frames. This can also introduce a significant error in the phase measurement if the non-linearity is large. The nonlinearity can introduce unequal phase shift only in one or more than one phase shifted frame keeping equal phase shift between rests of the frames. Even a small phase drift in only one of the frame will results into rather large reconstruction artefacts as seen in Fig. (1).

Next, effect of 'δ' on the phase measurement during reconstruction step using Eq. (6) is studied. The phase shift error 'α_t' is kept zero for this study. This is analogous to the situation in which prior information about the equal phase shift between data frames is unknown. It is observed

Optics EXPRESS

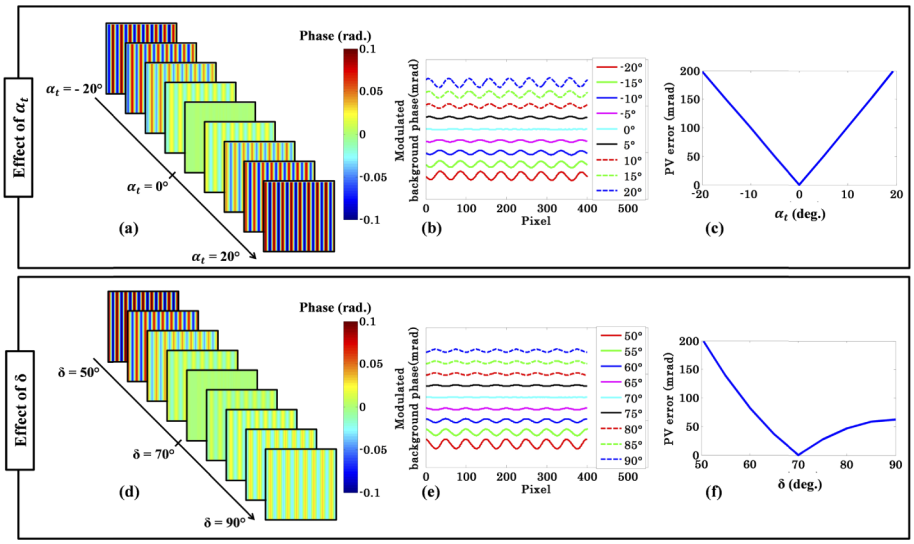

Fig. 1. Simulation results to understand the effect of phase shift 'δ' and phase shift error 'α' on the phase measurement. (a) Reconstructed phase map from the simulated five equal phase shifted plane wave interferograms except one, which have a range of phase shift error 'α_t' from – 20° to 20° at an interval of 5°. (b) Corresponding line profiles along white dotted line of reconstructed phase maps. (c) PV phase error as a function of phase shift 'α_t'. (d) Reconstructed phase map from the simulated five phase shifted (=70°) plane wave interferograms for a range of 'δ' from 50° to 90° at an interval of 5°, which are inserted into Eq. (6) during reconstruction. (e) Corresponding line profiles along white dotted line of reconstructed phase maps. (f) PV phase error as a function of 'δ'.

that use of wrong 'δ' rather than the actual phase shift value adopted by phase shifter may also introduce background modulation error during reconstruction as shown in Fig. 1(d). In order to realize it numerically, a range of phase shift 'δ' from 50° to 90° in a step of 5° is introduced in Eq. (6). The reconstructed phase maps corresponding to above range of 'δ' are presented in Fig. 1(d). Figure 1(e) depicts line profiles corresponding to all the reconstructed phase maps. Figure 1(f) illustrates the variation of maximum PV error as a function δ. It is evident from Figs. 1(c) and 1(f), that the variations of PV error as a function of 'α_t' and 'δ' are not the same. It is noteworthy that phase shift error 'α_t' and/or insertion of wrong value of 'δ' in Eq. (6) during reconstruction leads to the generation of serious modulated background phase error in the phase map. The phase error will even increases further if both the values ('α_t' and 'δ') are wrong during the reconstruction. If all the frames have 1° error in the phase shifts from the expected value, i.e., 70°. Then, peak-to-valley phase error and standard deviation is found to be equal to 0.0794 rad and 0.0255 rad, respectively.

2.2.2. Proposed phase shift measurement algorithm

Any phase shift 'δ' during reconstruction and/or any phase shift error 'α_t' during recording significantly affects the phase measurements as seen in Fig. (1). For an accurate phase measurement, it is necessary to effectively suppress the background phase error from the reconstructed phase maps. The conventional way of performing this is to use costly opto-mechanical components (such as SLM, PZT etc.) to introduce phase shifts between the interferograms. Here, we take an inverse approach where we allow phase to drift with time and record a continuous movie followed by a computational method which can extract five (or more) equally phase shifted interferograms for retrieval of the phase information. Here, a time lapsed

Optics EXPRESS

interferometric movie of the test object, which contains all the phase shifted interferograms (equal and unequal both), is recorded. The interferometric movie is further drag and drop into ImageJ software to extract all the frames of the movie. The unknown phase shifts between all the extracted frames make the accurate phase extraction difficult. Here we implemented Fourier transform based algorithm to calculate the phase shift between frames accurately, which enables the use of five frame phase shifting algorithm for accurate phase retrieval related to object.

To calculate the phase shift 'Δ' between phase shifted interferograms, following steps were adopted:

(1) Draw a line profile along a line perpendicular to the interference fringe pattern, where no object structure is present,

(2) Compute the wrapped phase map of the line profiles of the consecutive interferograms by employing Fourier transform based algorithm

(3) Zero padding is done to improve the accuracy in finding the position of Fourier peak.

(4) Unwrap the wrapped phase obtained from step (2) using built in MATLAB unwrap command.

(5) Calculate the phase difference 'Δ' between two consecutive interferogram by taking the difference between their phase values at a particular position as illustrated in Fig. 2(d).

(6) Finally, phase shifts of all the frames with respect to the first frame are calculated by following previous steps 1–5.

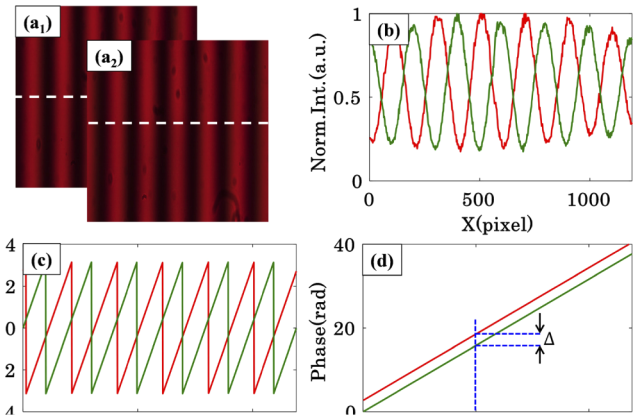

Fig. 2. Diagrammatical illustration of the sequence of steps followed in developed phase shift measurement algorithm.

The diagrammatical illustration of the sequence of steps above is presented in Fig. (2).

Figure 2(a) depicts two different interferograms having some unknown phase shift between them. To calculate phase shift between them line profiles were taken along the direction perpendicular to the fringe, i.e., white line for both interferograms shown in Fig. 2(a). The corresponding line profiles are presented in Fig. 2(b). Fourier transform based phase recovery algorithm is implemented to calculate the wrapped phase maps as depicted in Fig. 2(c) [4]. Finally, the wrapped phase is unwrapped by employing 1D phase unwrapping algorithm. The corresponding unwrapped phase maps are illustrated in Fig. 2(d). The difference between the phase values provide the information about the phase shift 'Δ' between the consecutive interferograms.

Optics EXPRESS

Currently, the proposed algorithm requires specimen-free region within the FOV of the phase microscope. However, the method can be extended such that the need of sample-free region is not needed in the future. It can be implemented by taking the intensity line profile at a particular pixel of the interferogram along the time axis of the movie. Then, the intensity versus time line profile can be used to measure the phase shift between the consecutive frames of the movie using either a Fourier transform of a Hilbert transform methods.

3. Materials and Methods

3.1. Experimental details

To realize the effect of equal and unequal phase shifted interferograms on the phase measurement experimentally, we employed white light phase shifting interference microscopy (WL-PSIM) as depicted in Fig. (3). Further, same optical setup is utilized to exhibit the capability of the proposed algorithm incorporated with five frame phase shifting algorithm for accurate phase measurement of optical waveguides and biological cells.

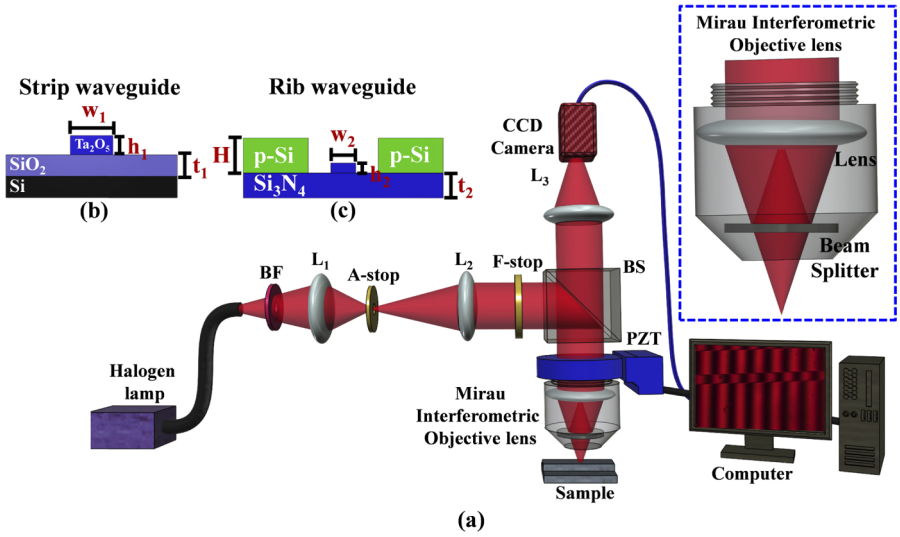

Fig. 3. (a) Schematic diagram of WL-PSIM setup. L_1, L_2 and L_3: lenses; BS: beam splitter; A-stop: aperture stop; F-stop: field stop; BF: bandpass filter; PZT: piezo electric transducer; and CCD: charge coupled device. Figure 1 b-c shows the schematic diagram of two optical waveguide geometries (b) strip, and (c) rib waveguides. Strip waveguide is made of Ta_2O_5: tantalum pentoxide (core), SiO_2: silicon di-oxide, Si: silicon substrate. Rib waveguide is made of Si3N4: silicon nitride (core), and p-Si: poly-silicon (absorbing layer). The waveguide parameters are w_1, w_2 = widths, h_1, h_2 = strip and rib height, t_1 = thickness of SiO_2, t_2 = slab region of rib waveguide and H = total thickness of absorbing layer. See Visualizations 1-3.

The experimental scheme of the present setup is based on the principle of white light interference microscopy. The narrow bandpass filter having peak wavelength 620 nm with ~ 40 nm spectral bandwidth is inserted into white light beam path for the recording spectrally filtered interferogram. The image of the light source is relayed at aperture stop (A-stop) plane using lens L_1, where size of aperture controls spatial coherence of the light source. The source image is further relayed at the back focal plane of the objective lens with the help of lens L_2 and beam splitter BS to achieve uniform illumination at the sample plane. The field stop (F-stop) controls the field of view (FOV) of the microscope. The beam splitter BS directs the beam towards

Optics EXPRESS

Mirau interferometric objective lens (50×/0.55 DI, WD 3.4 Nikon, Japan) to generate filtered white light interferograms easily (inset of Fig. (3)). More details about the Mirau interferometric objective lens can be found elsewhere [13,38]. The Mirau interferometer is attached with PZT to introduce required temporal phase shift between data frames. The phase shifted data frames are then captured using CCD/CMOS camera for further analysis.

3.2. Test sample

Two different optical waveguides and human blood are utilized as test specimens in the proposed work. The schematic diagrams of the optical waveguide geometries: strip and rib waveguide, are depicted in Figs. 3(b) – 3(c), respectively. Strip and rib waveguides were fabricated by sputtering a guiding layer of Ta_2O_5 [39] and Si_3N_4 [40] onto a silica (Si) substrate followed by photolithography and argon ion-beam milling, respectively [41]. For strip waveguides, the layer of Ta_2O_5 ($n_{core} = 2.12$ @ 620 nm) had a thickness 'h_1' of 220 nm and width 'w_1' of 10 µm, and was completely etched down to the SiO_2 layer (n = 1.45). For the rib waveguides, the layer of Si_3N_4 (refractive index ~ 2.041 at 620 nm) is only partially etched down by thickness 'h_2' leaving a final slab thickness of 't_2'. The rib region had a thickness 'h_2' of 8 nm and width 'w_2' of 2 µm. The rib waveguide had an absorbing layer (H = 180–200 nm) of poly-silicon (p-Si) onto Si_3N_4 as illustrated in Fig. 3(c). More details on the optimization of waveguide fabrication can be found elsewhere [39,40]. Strip waveguide geometry is utilized to realize the effect of phase shift error 'α_t' and phase shift between data frames 'δ' on the phase measurement. Same waveguide geometry is further used to compare the reconstructed phase maps obtained from manual phase shifting and well calibrated PZT. The rib waveguide geometry is employed to investigate the influence of shot noise on the system's phase measurement sensitivity.

For the preparation of biological sample, fresh blood sample is collected from a healthy donor with skin puncture. The fingertip is, first, cleaned with 70% isopropyl alcohol before the skin puncture. The skin is then punctured with one quick stroke to achieve a good flow of blood from the fingertip. The first blood drop is wiped away to avoid the excessive tissue fluid or debris. The surrounding tissues are gently pressed until another blood drop appears. The blood drop is then put onto the reflecting silicon substrate and spread using a glass slide to form a thin blood smear for interferometric recording.

4. Experimental results and discussion

4.1. Experimental realization of the influence of 'α_t' and 'δ' on the phase measurement

To experimentally realize the effect of 'α_t' and 'δ' on the phase measurement, experiments are conducted on an optical waveguide with stripe geometry. The strip waveguide was made of Ta_2O_5, of 220 nm thickness and 10 µm wide, others details are presented in section 3.2. The strip waveguide is placed under the WL-PSIM having 620 nm central wavelength bandpass filter (bandwidth ~ 40 nm) into the white light beam path to record a time lapsed movie of (frame rate ~15 fps) of the five phase shifted interferograms using uncalibrated PZT (see Visualization 1). For more details about the experimental setup see material and methods section. The interferometric movie of the waveguide is recorded without vibration isolation table under environmental fluctuation to capture phase shifted interferograms. The phase shifted interferograms were then extracted into frames using ImageJ software. The phase shifts between first and rest of the frames were, further, calculated by using the developed algorithm. Once the phase shifts between frames are measured, the following studies are performed experimentally: (1) the effect of phase shift 'δ' used at the time reconstruction and (2) effect of phase shift error 'α_t' which occurs due to PZT uncalibration or air turbulence/vibration.

The five equal phase shifted interferograms were selected from the recorded interferometric movie for the waveguide phase measurement. The frame numbers of the five phase shifted

Optics EXPRESS

interferograms were found to be 1, 49, 84, 129, 170 frames of the movie having phase shift between consecutive frames approximately equal to 70.8° using the developed algorithm. The precision in the phase shift step value 'δ' given in the consecutive frames depends on the fringe width of the interferogram. The fringe width of the interferogram is given in terms of the number of pixels covering one full fringe. Since in our experimental setting, one fringe of the interferogram is covering 212 pixels. Therefore, the width of single pixel (i.e., precision) in terms of phase values can be calculated using the following relation: $P = 2\pi/212$ rad. The precision in the phase shift step value 'δ' is calculated to be equal to 1.69°. Its value can be further reduced by covering more pixels in one fringe width of the interferogram.

Further, the above frames are utilized in Eq. (6) to measure the phase map of strip waveguide. Figure 4(a) depicts the reconstructed waveguide phase map having minimal background noise may be due to the detector's non-linear noise. The magnified view and corresponding line profile of background phase map (region enclosed by the red box) are shown in Fig. 4(b). It can be visualized from Fig. 4(b); PV phase shift error noise has been completely removed from the phase images. The phase noise of approximately 30 mrad could be present due to the detector's noise and shot noise. The mathematical formulation of the effect of shot noise on the spatial phase sensitivity of the system is presented in section 4.3.

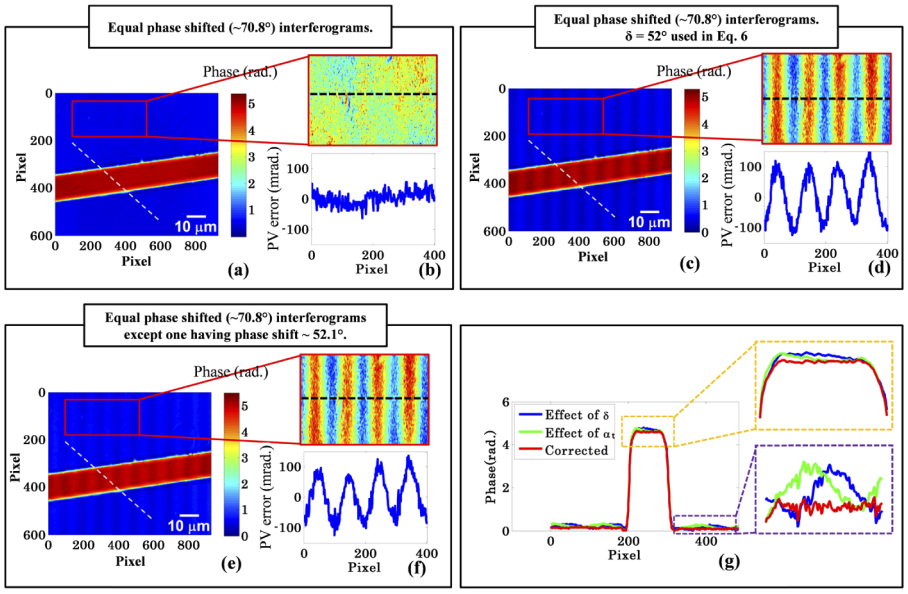

Fig. 4. Experimental investigation of the effect of phase shift 'δ' and phase shift error 'α_t' on the quantitative measurement of optical waveguide. The test sample is stripe waveguide of 220 nm height. (a) Reconstructed waveguide phase map when all five equal phase shifted (~70.8°) interferograms obtained from the proposed algorithm are utilized for the reconstruction. (b) Line profile along black dotted line shown in the inset of (a). (c) Reconstructed waveguide phase map when the value of 'δ' equal to 52° instead of 70.8° is utilized during reconstruction using Eq. (6). (d) Line profile along black dotted line shown in the inset of (c). (e) Reconstructed waveguide phase map when all five equal phase shifted (~70.8°) interferograms except one which have a phase shift value equal to 52.1° instead of 70.8° are utilized for the reconstruction. The value of 'δ' equal to 70.8° is used in Eq. (6) for the reconstruction. (f) Line profile along black dotted line shown in the inset of (e). (g) Line profile along white dotted lines shown in (a, c, e). The scale bar is depicted in white color line.

Optics EXPRESS

To envisage the influence of wrong 'δ' on the phase measurement of waveguide, the value of $\delta = 52°$ is put into Eq. (6). The same frames given above are utilized for the reconstruction. The PV value of background modulation is much smaller than the maximum phase value of waveguide. Therefore, $\delta = 52°$ is chosen to clearly visualize the background modulation with waveguide phase map as illustrated in Fig. 4(c). The reconstructed phase map of waveguide when $\delta = 52°$ instead of actual phase shift (i.e., 70.8°) is used in Eq. (6) is shown in Fig. 4(c). The background modulation can be clearly visualized in the reconstructed waveguide phase map as depicted in the magnified view of Fig. 4(c). Figure 4(d) shows the line profile along black dotted line in the enlarged region of Fig. 4(c) as marked with the red box. The PV error generated in the reconstructed phase map is found to be equal to 200 mrad at $\delta = 52°$ (Fig. 4(d)), which is in a close agreement with the simulation results.

Similarly, to investigate the effect of phase shift error 'α_t' on the reconstructed phase map, one of the interferometric frame say 49th (phase shift ~ 70.8°) is being replaced from 77th frame (phase shift ~ 52.1°). Figure 4(e) illustrates 2D reconstructed phase map of the waveguide, when one of the interferogram having phase shift equal to 52.1° is used keeping other phase shifted frames same. This situation is analogous to simulated ones, where unequal phase shift is intentionally introduced into one of the phase shifted interferogram (Fig. 1(b)). The unequal phase shift between above two frames (1st and 77th) is originated because of the external vibration, hysteresis and nonlinearity of PZT. The insets of Figs. 4(c) and 4(e) are the magnified images of background phase map marked with red boxes. Figure 4(f) presents line profile along the black dotted line. It is illustrated from Fig. 4(f); sinusoidal background phase error is generated while using one unequal and rest of the equal phase shifted interferograms in five frame phase shifting algorithm [in Eq. (6)]. It is quite evident from Figs. 4(d) and 4(f), PV errors in both the cases are found to be equal to ~ 200 mrad, which exhibit a good agreement with the simulated results. It is therefore necessary to have equal phase steps (i.e. $\alpha_t = 0$) and accurate determination of phase shift between frames (i.e., precise δ).

To further compare noise level of the corrected phase map with the reconstructed ones under the influence of 'δ' and 'α_t', line profiles were plotted along white dotted lines shown in Figs. 4(a), 4(c), 4(e). It can be envisaged from Fig. 4(g), wrong 'δ' during reconstruction and phase shift error 'α_t' during recording greatly influence the phase measurement of test object. The insets of Fig. 4(g) depict this in the magnified views of line profiles marked with dotted yellow and purple boxes.

4.2. A comparison of proposed method and PZT assisted QPI of optical waveguide

To demonstrate the robustness of the proposed method instead of using piezo-translation stages two simple methods are used to induce the phase shift. First a simple manual translation of reference or sample arm and second by using hair dryer to introduce random phase shift. Both the methods worked equally well but in the present work we included results obtained from manual phase shifting technique. The recorded interferometric movies of the temporal phase shifted frames introduced by hair dryer (Visualization 2) and translation of reference or sample arm manually (Visualization 3) can be found in supplementary video. Temporal phase shift introduced due to the translation of sample arm manually is utilized for quantitative imaging of a strip optical waveguide and liver sinusoidal endothelial cells (LSECs).

To demonstrate the phase measurement accuracy while using manual phase shifting technique, results are compared to that of well calibrated PZT. Figures 5(a) and 5(b) are the results obtained from well calibrated PZT of a stripe optical waveguide (H = 220 nm). One of the phase shifted interferogram recorded by employing WL-PSIM and calibrated PZT is illustrated in Fig. 5(a). The equal five phase shifted frames (phase shift ~ 75°) are further utilized for the reconstruction of phase map of strip waveguide as depicted in Fig. 5(b).

Optics EXPRESS

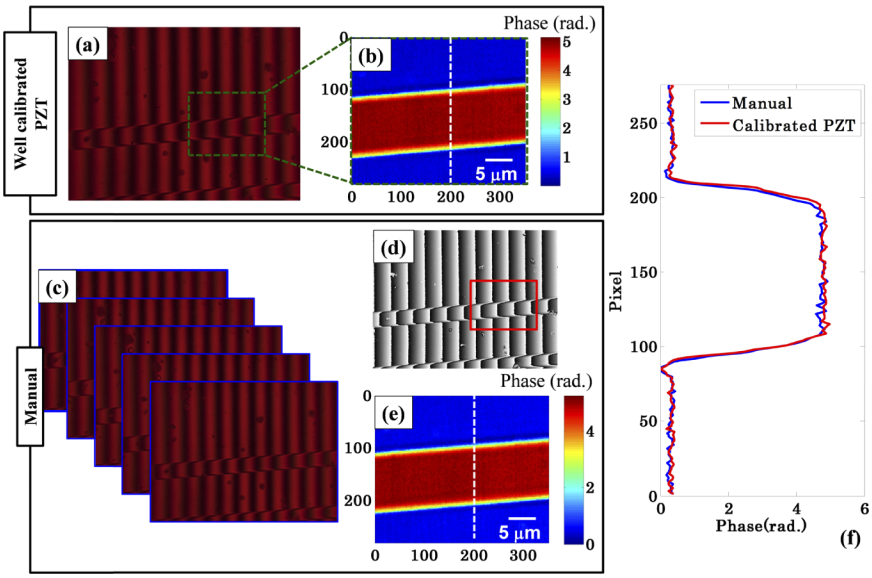

Fig. 5. Quantitative phase measurement of optical waveguide using calibrated PZT and unconventionally obtained temporal phase shifted interferograms, which is done by the translation of sample stage manually. The test sample is stripe waveguide of 220 nm height. (a) One of the five equal phase shifted interferogram of optical waveguide obtained from calibrated PZT. (b) Corresponding unwrapped phase map. (c) Five equal phase shifted interferograms of waveguide extracted from a recorded movie using proposed algorithm. (d) Corresponding wrapped phase map. (e) Unwrapped phase map of the region marked with red box. (f) Line profiles along white dotted vertical lines illustrated in (b) and (e). The scale bar is depicted in white color.

To verify the capabilities of proposed algorithm, experiments are performed on the same waveguide. A continuous temporal phase shift in the interference pattern is introduced by translating sample stage manually. The time lapsed interferometric movie of waveguide is then recorded using Infinity2-1RC color CCD camera having frame rate ~ 15 fps (see Visualization 3). Using the proposed methodology (as discussed in Section 3.2) the measurement of phase shift between data frames was determined. The five equal phase shifted (phase shift ~ 69°) interferometric frames are selected from the recorded movie as shown in Fig. 5(c). These extracted five phase shifted frames are then utilized to calculate wrapped phase map using Eq. (6). To determine unwrapped phase map related to waveguide, a minimum L^P norm 2D phase unwrapping algorithm is applied [42]. The 2D reconstructed phase map corresponding to the region enclosed by red box is presented in Fig. 5(e). To compare the reconstructed phase maps obtained from manual phase shifting and well calibrated PZT, line profiles along the white dotted lines shown in Figs. 5(b) (calibrated PZT) and 5(e) (manual) are drawn as presented in Fig. 5(f). It is worth noting from Fig. 5(f) that phase maps correspond to calibrated PZT and manual phase shifting are found to be in close agreement with each other. The noise generated in the reconstructed phase maps is due to the camera noise.

4.3. QPI of thin optical waveguide and comparison with AFM

To exhibit the potential of the present technique in terms of height measurement accuracy, experiment is performed on a Si_3N_4 rib waveguide with rib height of only 8 nm and further compared with Atomic force microscopy (AFM) result. The small rib height of 8 nm corresponds

Optics EXPRESS

to an optical height ~ 8.16 nm at 620 nm wavelength. Additional details of the rib waveguide can be found in section 3.2.

To investigate the height measurement accuracy of the present approach, the rib waveguide is placed under the WL-PSIM having 620 nm central wavelength bandpass filter (bandwidth ~ 40 nm) into the white light beam path to record temporally phase shifted interferograms manually at ~ 34 fps (see Visualization 4). Thus, only 6s interferometric movie is sufficient to provide ~ 200 data frames while employing CMOS camera (C11440-36U). The interferometric movie contains phase shifted interferograms, which are extracted into individual frames using ImageJ software. The phase shifts between first and rest of the frames are then calculated by using the proposed algorithm. Once the phase shifts between frames are measured, the equal five phase shifted frames are selected for the calculation of the phase map of waveguide by employing Eq. (6). The five equal phase shifted interferograms corresponds to the frames 1, 56, 89, 134, and 171 having phase shift equal to 84.9°.

Figure 6(a) represents one of the interferogram from the set of five phase shifted interferograms. The recovered phase map is illustrated in Fig. 6(b). It can be visualized from the retrieved phase map that the background modulation is not observed. The recovered phase map shows narrow rib waveguide (of 8 nm rib height) along the middle line of blue color region (Fig. 6(b)), which is otherwise difficult to visualize in the interferometric images. Figure 6(c) illustrates the magnified view of the region of Fig. 6(b) marked with green dotted boxes having 8 nm rib height. The enlarged phase map is further used to measure corresponding height map as shown in Fig. 6(d) using Eq. (7). The line profiles of retrieved phase and height maps along white dotted lines are depicted in Figs. 6(e) and 6(f).

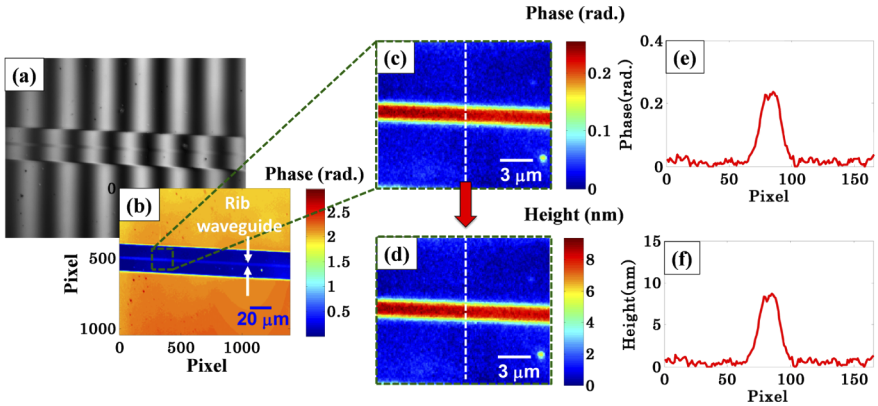

Fig. 6. Quantitative phase/height measurement sensitivity of the present method while using 12-bit monochrome CMOS camera. The specimen is shallow rib waveguide of rib height of only 8 nm. Five temporally phase shifted interferograms are extracted using ImageJ from a movie recorded by the translation of sample stage manually (see Visualization 4). (a) One of the phase shifted interferograms of rib waveguide extracted from a movie recorded by 12-bit monochrome CMOS camera using proposed algorithm. (b) Corresponding unwrapped phase map. (c, d) Unwrapped phase and height map of the region marked with green dotted box in (b). (e, f) corresponding line profiles of 8 nm rib waveguide along white dotted vertical lines. The scale bars are depicted in blue and white colors. See Visualization 4.

The peak to valley (PV), mean and standard deviation (SD) of the phase noise are found to be equal to 37.40, 13.14, 8.3 mrad, respectively. The theoretical phase sensitivity is calculated by the following relation [43]:

$$\Delta\phi = \pi \Big/ 2V\sqrt{P} \tag{8}$$

Optics EXPRESS

Where, P is equal to the total number of photoelectrons detected during one fringe of the interferogram. V is the visibility of the interferogram and can be calculated using the following relation:

$$V = \frac{I_{max} - I_{min}}{I_{max} + I_{min}} \tag{9}$$

I_{max} and I_{min} are the maximum and minimum intensity values of the interferogram.

The visibility of the interferogram is calculated to be equal to 0.47. The total number of photoelectrons detected during one fringe of the interferogram is approximately 275665. If we use these numbers in Eq. (8), then the theoretical phase sensitivity is found be equal to 6.3 mrad. The experimental phase sensitivity is 8.3 mrad. The experimental value of the phase sensitivity is found to be in a good agreement with the theoretical one. In the proposed work, the full well capacity of the detector is not utilized, which is around 33000 e- due to the less intensity in our filtered white light source. The phase sensitivity of our system can be further improved by utilizing the full well capacity of the detector.

The height of the rib waveguide is measured to be equal to $\sim 8.1 \pm 0.4$ nm, which is found to be in a close agreement with the value obtained from AFM (Bruker Dimension icon), see Fig. (7). The height of the rib waveguide measured by AFM is found to be equal to $\sim 7.5 \pm 0.2$ nm. The 3D height map of the same rib waveguide is illustrated in Fig. 7(a). The line profile of the height map along the green dotted line is depicted in Fig. 7(b). The slight inaccuracy ~ 0.5 nm in the height measurement could be arising due to the following possible reasons: (1) small variations of height for rib waveguide of rib height of 8 nm, (2) detector's noise/shot noise, and (3) measurement inaccuracy of AFM (~ 0.6 nm). The measurement error due to detector's noise can be further corrected with the implementation of less noisy 16-bit or cooled CCD/CMOS camera for interferometric recordings, which can be more explored in future. It is worth noting that detector's noise/shot noise greatly influence the height measurement accuracy of the test specimens especially for the objects having small optical thickness.

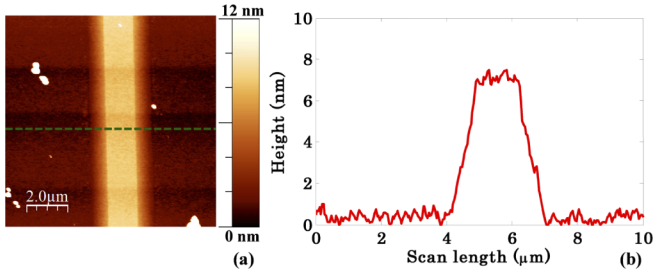

Fig. 7. Profilometry of 8 nm optical rib waveguide using Atomic Force Microscopy. (a) Height map of rib waveguide. (b) Corresponding line profile along the green dotted horizontal line.

4.4. QPI of extremely thin optical waveguide and biological specimens

To demonstrate the capability of the present method in terms of optical path length (OPL) sensitivity, experiments are performed on a Si_3N_4 rib waveguide with rib height of only 2 nm and LSECs (H $\sim$ 100 nm). The small rib height of 2 nm generates very small optical height $\sim$ 2.04 nm at 620 nm wavelength. Due to small OPL, such samples are difficult to realize under conventional DHM due to coherent noise of laser. Further, conventional WL-PSIM for the phase measurement suffers from the issues of hysteresis and nonlinearity of PZT, and environmental instability.

First, the experiment was performed on optical waveguide with rib height of only 2 nm and width of 100 μm (Fig. 8(a)). The movie containing temporally phase shifted interferograms of

Optics EXPRESS

waveguide with rib height of only 2 nm is recorded by following the previous scheme and can be found in supplementary video (see Visualization 5). The five frames which have equal phase shift (~72°) between consecutive frames are found to be 1, 24, 32, 49, and 71 frames of the movie. One of the five equal phase shifted interferogram is shown in Fig. 8(b). The extracted data frames are further utilized to measure the height map of 2 nm rib waveguide. The inset illustrates the magnified view of the region marked with red dotted box in Fig. 8(b) having 2 nm rib height lies between two blue color dotted horizontal lines. The segmented region marked with red dotted box in Fig. 8(b) is further used to measure corresponding height map using Eq. (7) as depicted in Fig. 8(c). The line profile of retrieved height map along black dotted line is depicted in Fig. 8(d). The height of the rib waveguide is measured to be equal to $\sim 2.3 \pm 0.3$ nm, which is in a close agreement with the actual value ~ 2 nm. The slight inaccuracy could be again due to the detector's noise/shot noise.

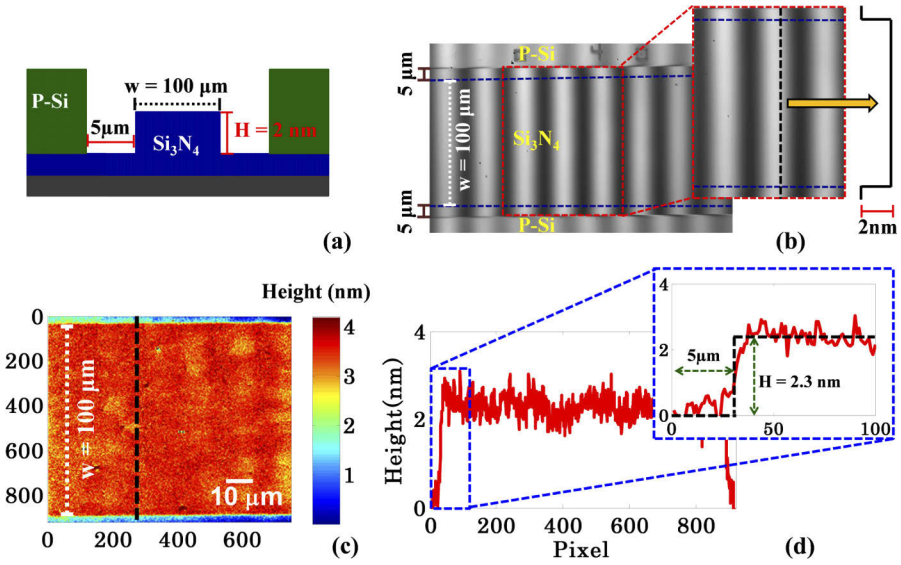

Fig. 8. Height measurement of 2 nm rib waveguide while using monochrome CMOS camera. (a) Rib waveguide structure. (b) One of the phase shifted interferogram of rib waveguide. (c) Corresponding height map. (d) The line profile of 2 nm rib waveguide along black dotted vertical line. The scale bar is depicted in white color. See Visualization 5.

Next, QPI of mice LSECs [44] (H ~ 100 nm) is done to demonstrate the capability of the proposed method in the field of biomedical imaging. The membrane of these cells is very thin and generates small change in the wavefront of the interacting light beam. The optical path difference between the cell (n_{cell} ~1.38) and the outside medium (n_m ~1.33) is of the order of ~ 5 nm due to the low refractive index contrast between them. A Linnik interference microscopy system is employed to image these cells. The details of the experimental system can be found in Ref. [45]. The experimental scheme depicted in Fig. (3) is not implemented to image LSECs. This is due to the limitation of Mirau based WL-PSIM, where the reference mirror is fixed inside the interference objective lens. Therefore, it does not provide interference between the object and the reference beams when implemented to image biological objects surrounded by the liquid medium. The biological medium surrounding the object introduces extra optical path length in the object arm which cannot be corrected due to the fixed reference mirror. This exhibits that the proposed method can be implemented with any QPM system. This is not only limited to the experimental scheme shown in Fig. (3).

Optics EXPRESS

A time lapse interferometric movie of LSECs can be seen in Visualization 6. The continuous phase shift between data frames is introduced manually. The recorded movie is extracted into frames using ImageJ software. Then developed algorithm is adopted to identify equal five phase shifted interferograms/frames of LSECs. Figures 9(a) and 9(b) shows bright field image and corresponding five phase shifted interferograms of LSECs, respectively. The wrapped phase map of LSECs is further calculated using five frame phase shifting algorithm Eq. (6) and illustrated in Fig. 9(c). The phase ambiguities are removed by employing minimum L^P norm 2D phase unwrapping algorithm [42]. The reconstructed phase map of LSECs is depicted in Fig. 9(d). It can be seen that 2D phase map of LSECs does not have sinusoidal background phase error.

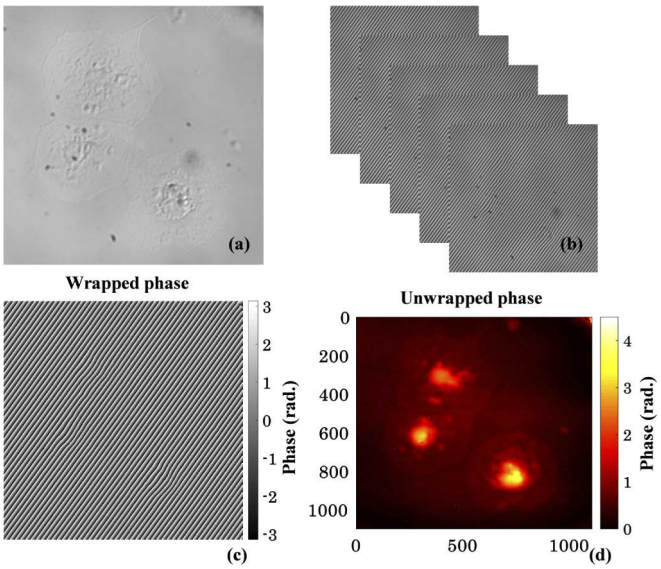

Fig. 9. Quantitative phase measurement of LSECs using unconventionally obtained temporal phase shifted interferograms, which is done by translating the sample stage manually. (a) Bright field image. (b) Five equal phase shifted interferograms of LSECs extracted from a recorded movie using proposed algorithm. (c) Corresponding wrapped phase map. (d) Unwrapped phase map. The scale bar is depicted in black color. See Visualization 6.

4.5. *Comparative study of 'α_t' and 'δ' for QPI on thin and thick structures*

PSI has been extensively used for the QPI of various biological cells/tissues such as RBCs, HeLa cells, macrophages and cancer tissues in the past [46–49]. However, the influence of either phase shift error 'α_t' or wrong 'δ' on their reconstructed phase maps has not been taken care of previously. The modulated background phase error (~ 100–200 mrad.) might not be crucial for the phase objects having height 2–4 μm (or $\varphi \sim 2$–10 rad.), such as RBCs. Although, it will introduce some sort of measurement error in their reconstructed phase maps. Whereas, such modulated phase error can be a big problem for the specimens having small optical thickness (2–100 nm) such as shallow rib waveguide and LSECs as discussed in this work or other thin structures such as tail of sperm cells [50] and E. coli bacteria [51] etc.

We carried out a systematic study on two structures having different thicknesses to envisage the influence of background modulation. First structure having relatively large thickness, i.e. human RBCs (thickness of around ~2.5 micron) and second structure having small thickness, i.e. optical waveguide with rib height of only 8 nm are utilized during experiments. Figures 10(a) and 10(d) depict the reconstructed phase maps of human RBCs and rib waveguide, respectively, without

Optics EXPRESS

modulation error. It can be clearly visualized from Figs. 10(b) and 10(c) that the background modulation generated due to phase shift error 'α_t' of 12° and utilization of wrong phase shift value 'δ' equal to 74° instead of its actual value (i.e., 86°) is not visible with RBCs phase map. Whereas, it is found to be indispensable for 8 nm rib waveguide and affects the results significantly as presented in Figs. 10(e) and 10(f). It is worth noting that the background modulation error generated due to α_t = 12° and phase shift value 'δ' equal to 72° rather than its actual value (i.e., 84°) greatly influence the reconstructed phase map of 8 nm rib waveguide.

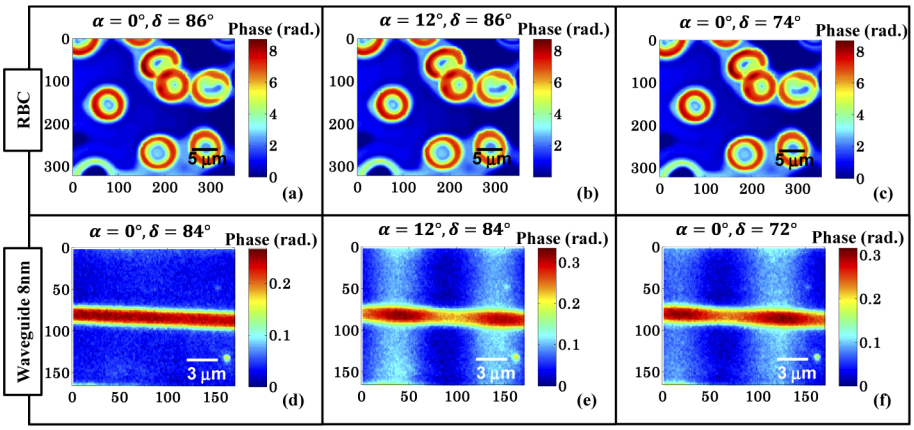

Fig. 10. Investigation of the influence of phase shift error 'α_t = 12°' and wrong 'δ' on QPI of human RBCs and 8 nm rib waveguide. A small error in α_t and δ does not influence the phase images of RBC (2.5 μm thickness), while it generates strong modulation in the phase images of rib waveguide having thickness of 8 nm.

5. Conclusion

Here, we demonstrate that a slight phase shift error (α_t) introduces an unwanted background modulation in the reconstructed phase map. Similar type of modulation is also observed in the reconstruction when wrong value of phase shift 'δ' is utilized in Eq. (6). Experimentally, there are various possible reasons behind the phase shift errors such as hysteresis and nonlinearity of PZT, environmental instability and unwanted vibrations in the set-up. In order to avoid these problems, a time lapsed interferometric movie of temporally phase shifted frames is recorded. The interferometric movie contains all equal and unequal phase shifted interferograms. However, phase shift between all the data frames are unknown. A new numerical algorithm is proposed that can calculate the amount of phase shift between all frames of movie with high precision ≤ 5.5 $\times 10^{-4}$ π rad. Five equally phase shifted images from the movie is then extracted to generate uncompromised quantitative phase image of the samples. Using the proposed methodology, the phase sensitivity is found to be minimal (< 1 nm) while using 12-bit CMOS camera for interferometric recording. The phase sensitivity/accuracy of the PSI techniques can be further improved with the utilization of 16-bit super-cooled camera. We also demonstrated the influence of detector's noise/shot noise on the phase measurement sensitivity which becomes prominent on specimen having small optical thickness (< 10 nm).

The proposed way of recording temporal phase shifted interferograms and phase shift calculation algorithm can be applied under the influence of vibration/ air turbulence. The accuracy of the phase map reconstruction is found to be in close agreement to that of well calibrated PZT. The proposed approach has the capability to enable many unconventional methods like translation of reference or sample arm manually, natural vibrations/air turbulence, cell phone vibration,

Optics EXPRESS

and artificial air turbulence generated from hair dryer etc. for introducing temporal phase shift between data frames.

The PSI has mostly implemented for the phase imaging of thick biological/wavguide samples such as RBCs, HeLa cells, macrophages and cancer tissues previously, where minute phase variation will not be visible [46–49]. Therefore, background modulation (100–200 mrad.) would be difficult to see along with thick sample's phase map (2–4 rad.). Here, we demonstrated that a slight phase shift error (such as '$\alpha_t = 12°$') or utilization of wrong 'δ' is crucial in PSI for the accurate phase/height measurements of objects having sub-10 nm height. The origin and the complete removal of these modulated background error on objects having small thickness (<10 nm) were unaddressed previously.

By using the proposed methodology we successfully measured 2 nm rib height of an optical waveguide with a background noise of 4 Å. Interestingly these measurements were done without using any PZT in presence of environmental fluctuations. The proposed method will find application in QPI of biological cells and tissues without any priori calibration of phase shifts and applications where QPI of optical trapped or propelled objects are required [52–54]. Thus, the proposed method can be implemented in a robust environment without using any vibration isolation optical tables and PZT. The time requirement for obtaining five equal phase shifted frames from set of large number of frames (e.g. 200) can be reduced by using high-speed camera. For instance a high speed camera operating at 1000 fps will record 200 frames in only 0.05–0.2 second. Thus, the present technique can be further extended to the phase imaging of moving living cells or sub-cellular structures [1,3,55].

Funding

Department of Atomic Energy, Government of India (financial grant no. 34/14/07/BRNS); FP7 Ideas: European Research Council (project number 336716)); Direktoratet for internasjonalisering og kvalitetsutvikling i høgare utdanning ((Project number INCP- 2014/10024).); Norges Forskningsråd (BIOTEK 2021 – 285571)., NANO 2021 – 288565)).

Acknowledgements

The authors would like to acknowledge Dr. Peter Anthony Gerard McCourt and Karolina Szafranska for providing mice liver sinusoidal endothelial cells (LSECs).

Disclosures

The authors declare no conflicts of interest.

References

1. M. K. Kim, *Digital Holographic Microscopy: Principles, Techniques, and Applications* (Springer New York, 2011).
2. F. Charrière, A. Marian, F. Montfort, J. Kuehn, T. Colomb, E. Cuche, P. Marquet, and C. Depeursinge, "Cell refractive index tomography by digital holographic microscopy," Opt. Lett. **31**(2), 178–180 (2006).
3. B. Kemper and G. von Bally, "Digital holographic microscopy for live cell applications and technical inspection," Appl. Opt. **47**(4), A52–A61 (2008).
4. M. Takeda, H. Ina, and S. Kobayashi, "Fourier-transform method of fringe-pattern analysis for computer-based topography and interferometry," J. Opt. Soc. Am. A **72**(1), 156–160 (1982).
5. P. Hariharan, B. Oreb, and T. Eiju, "Digital phase-shifting interferometry: a simple error-compensating phase calculation algorithm," Appl. Opt. **26**(13), 2504–2506 (1987).
6. K. Lee, K. Kim, J. Jung, J. Heo, S. Cho, S. Lee, G. Chang, Y. Jo, H. Park, and Y. Park, "Quantitative phase imaging techniques for the study of cell pathophysiology: from principles to applications," Sensors **13**(4), 4170–4191 (2013).
7. A. Ahmad, V. Dubey, G. Singh, V. Singh, and D. S. Mehta, "Quantitative phase imaging of biological cells using spatially low and temporally high coherent light source," Opt. Lett. **41**(7), 1554–1557 (2016).
8. F. Yi, I. Moon, and B. Javidi, "Cell morphology-based classification of red blood cells using holographic imaging informatics," Biomed. Opt. Express **7**(6), 2385–2399 (2016).
9. M. K. Kim, "Principles and techniques of digital holographic microscopy," J. Photonics Energy **1**(1), 018005 (2010).
10. H. Schreiber and J. H. Bruning, "Phase shifting interferometry," *Optical Shop Testing*, 3rd Edition, 547–666 (2006).

Optics EXPRESS

11. P. Sandoz, "An algorithm for profilometry by white-light phase-shifting interferometry," J. Mod. Opt. **43**(8), 1545–1554 (1996).
12. K. Creath, "V phase-measurement interferometry techniques," Prog. Opt. **26**, 349–393 (1988).
13. D. Singh Mehta and V. Srivastava, "Quantitative phase imaging of human red blood cells using phase-shifting white light interference microscopy with colour fringe analysis," Appl. Phys. Lett. **101**(20), 203701 (2012).
14. J. Li, L. Zhong, S. Liu, Y. Zhou, J. Xu, J. Tian, and X. Lu, "An advanced phase retrieval algorithm in N-step phase-shifting interferometry with unknown phase shifts," Sci. Rep. **7**(1), 44307 (2017).
15. J. Xu, Y. Li, H. Wang, L. Chai, and Q. Xu, "Phase-shift extraction for phase-shifting interferometry by histogram of phase difference," Opt. Express **18**(23), 24368–24378 (2010).
16. F. Liu, Y. Wu, and F. Wu, "Correction of phase extraction error in phase-shifting interferometry based on Lissajous figure and ellipse fitting technology," Opt. Express **23**(8), 10794–10807 (2015).
17. Y.-Y. Cheng and J. C. Wyant, "Phase shifter calibration in phase-shifting interferometry," Appl. Opt. **24**(18), 3049–3052 (1985).
18. N. Warnasooriya and M. K. Kim, "Quantitative phase imaging using three-wavelength optical phase unwrapping," J. Mod. Opt. **56**(1), 67–74 (2009).
19. C. Zhang, H. Zhao, L. Zhang, and X. Wang, "Full-field phase error detection and compensation method for digital phase-shifting fringe projection profilometry," Meas. Sci. Technol. **26**(3), 035201 (2015).
20. H. Zhang, M. J. Lalor, and D. R. Burton, "Error-compensating algorithms in phase-shifting interferometry: a comparison by error analysis," Opt. Lasers Eng. **31**(5), 381–400 (1999).
21. J. Schwider, R. Burow, K.-E. Elssner, J. Grzanna, R. Spolaczyk, and K. Merkel, "Digital wave-front measuring interferometry: some systematic error sources," Appl. Opt. **22**(21), 3421–3432 (1983).
22. P. Carré, "Installation et utilisation du comparateur photoélectrique et interférentiel du Bureau International des Poids et Mesures," Metrologia **2**(1), 13–23 (1966).
23. X. Xu, L. Cai, Y. Wang, X. Yang, X. Meng, G. Dong, X. Shen, and H. Zhang, "Generalized phase-shifting interferometry with arbitrary unknown phase shifts: direct wave-front reconstruction by blind phase shift extraction and its experimental verification," Appl. Phys. Lett. **90**(12), 121124 (2007).
24. G. Lai and T. Yatagai, "Generalized phase-shifting interferometry," J. Opt. Soc. Am. A **8**(5), 822–827 (1991).
25. P. Gao, B. Yao, N. Lindlein, K. Mantel, I. Harder, and E. Geist, "Phase-shift extraction for generalized phase-shifting interferometry," Opt. Lett. **34**(22), 3553–3555 (2009).
26. J. Vargas, J. A. Quiroga, and T. Belenguer, "Phase-shifting interferometry based on principal component analysis," Opt. Lett. **36**(8), 1326–1328 (2011).
27. Z. Wang and B. Han, "Advanced iterative algorithm for phase extraction of randomly phase-shifted interferograms," Opt. Lett. **29**(14), 1671–1673 (2004).
28. J. Vargas, C. Sorzano, J. Estrada, and J. Carazo, "Generalization of the principal component analysis algorithm for interferometry," Opt. Commun. **286**, 130–134 (2013).
29. J. F. Mosiño, M. Servin, J. Estrada, and J. Quiroga, "Phasorial analysis of detuning error in temporal phase shifting algorithms," Opt. Express **17**(7), 5618–5623 (2009).
30. J. C. Estrada, M. Servin, and J. A. Quiroga, "A self-tuning phase-shifting algorithm for interferometry," Opt. Express **18**(3), 2632–2638 (2010).
31. J. Vargas, J. A. Quiroga, C. Sorzano, J. Estrada, and J. Carazo, "Two-step demodulation based on the Gram–Schmidt orthonormalization method," Opt. Lett. **37**(3), 443–445 (2012).
32. J. Vargas, J. A. Quiroga, C. Sorzano, J. Estrada, and J. Carazo, "Two-step interferometry by a regularized optical flow algorithm," Opt. Lett. **36**(17), 3485–3487 (2011).
33. T. Tahara, Y. Awatsuji, Y. Shimozato, T. Kakue, K. Nishio, S. Ura, T. Kubota, and O. Matoba, "Single-shot polarization-imaging digital holography based on simultaneous phase-shifting interferometry," Opt. Lett. **36**(16), 3254–3256 (2011).
34. D. Abdelsalam, B. Yao, P. Gao, J. Min, and R. Guo, "Single-shot parallel four-step phase shifting using on-axis Fizeau interferometry," Appl. Opt. **51**(20), 4891–4895 (2012).
35. S. Jiao and W. Zou, "High-resolution parallel phase-shifting digital holography using a low-resolution phase-shifting array device based on image inpainting," Opt. Lett. **42**(3), 482–485 (2017).
36. T. Chen and C. Chen, "An instantaneous phase shifting ESPI system for dynamic deformation measurement," in *Optical Measurements, Modeling, and Metrology*, Volume 5 (Springer, 2011), pp. 279–283.
37. J. H. Bruning, D. R. Herriott, J. Gallagher, D. Rosenfeld, A. White, and D. Brangaccio, "Digital wavefront measuring interferometer for testing optical surfaces and lenses," Appl. Opt. **13**(11), 2693–2703 (1974).
38. A. Ahmad, V. Srivastava, V. Dubey, and D. Mehta, "Ultra-short longitudinal spatial coherence length of laser light with the combined effect of spatial, angular, and temporal diversity," Appl. Phys. Lett. **106**(9), 093701 (2015).
39. B. S. Ahluwalia, A. Z. Subramanian, O. G. Hellso, N. M. Perney, N. P. Sessions, and J. S. Wilkinson, "Fabrication of submicrometer high refractive index Tantalum Pentoxide waveguides for optical propulsion of microparticles," IEEE Photonics Technol. Lett. **21**(19), 1408–1410 (2009).
40. J.-C. Tinguely, ØI Helle, and B. S. Ahluwalia, "Silicon nitride waveguide platform for fluorescence microscopy of living cells," Opt. Express **25**(22), 27678–27690 (2017).
41. S. M. Lindecrantz and O. G. Hellesø, "Estimation of propagation losses for narrow strip and rib waveguides," IEEE Photonics Technol. Lett. **26**(18), 1836–1839 (2014).

Optics EXPRESS

42. D. C. Ghiglia and L. A. Romero, "Minimum Lp-norm two-dimensional phase unwrapping," J. Opt. Soc. Am. A **13**(10), 1999–2013 (1996).
43. J. C. Wyant, "Use of an ac heterodyne lateral shear interferometer with real–time wavefront correction systems," Appl. Opt. **14**(11), 2622–2626 (1975).
44. L. Wang, X. Wang, G. Xie, L. Wang, C. K. Hill, and L. D. DeLeve, "Liver sinusoidal endothelial cell progenitor cells promote liver regeneration in rats," J. Clin. Invest. **122**(4), 1567–1573 (2012).
45. A. Ahmad, T. Mahanty, V. Dubey, A. Butola, B. S. Ahluwalia, and D. S. Mehta, "Effect on the longitudinal coherence properties of a pseudothermal light source as a function of source size and temporal coherence," Opt. Lett. **44**(7), 1817–1820 (2019).
46. Y. Baek, K. Lee, J. Yoon, K. Kim, and Y. Park, "White-light quantitative phase imaging unit," Opt. Express **24**(9), 9308–9315 (2016).
47. S. Chen, C. Li, and Y. Zhu, "Low-coherence wavelength shifting interferometry for high-speed quantitative phase imaging," Opt. Lett. **41**(15), 3431–3434 (2016).
48. H. Majeed, M. E. Kandel, K. Han, Z. Luo, V. Macias, K. V. Tangella, A. Balla, and G. Popescu, "Breast cancer diagnosis using spatial light interference microscopy," J. Biomed. Opt. **20**(11), 111210 (2015).
49. Q. Zhang, L. Zhong, P. Tang, Y. Yuan, S. Liu, J. Tian, and X. Lu, "Quantitative refractive index distribution of single cell by combining phase-shifting interferometry and AFM imaging," Sci. Rep. **7**(1), 2532 (2017).
50. M. Haifler, P. Girshovitz, G. Band, G. Dardikman, I. Madjar, and N. T. Shaked, "Interferometric phase microscopy for label-free morphological evaluation of sperm cells," Fertil. Steril. **104**(1), 43–47.e2 (2015).
51. Y. Cotte, F. Toy, P. Jourdain, N. Pavillon, D. Boss, P. Magistretti, P. Marquet, and C. Depeursinge, "Marker-free phase nanoscopy," Nat. Photonics **7**(2), 113–117 (2013).
52. B. S. Ahluwalia, P. Løvhaugen, and O. G. Hellesø, "Waveguide trapping of hollow glass spheres," Opt. Lett. **36**(17), 3347–3349 (2011).
53. P. Løvhaugen, B. S. Ahluwalia, T. R. Huser, and O. G. Hellesø, "Serial Raman spectroscopy of particles trapped on a waveguide," Opt. Express **21**(3), 2964–2970 (2013).
54. A. Ahmad, V. Dubey, V. R. Singh, J.-C. Tinguely, C. I. Øie, D. L. Wolfson, D. S. Mehta, P. T. So, and B. S. Ahluwalia, "Quantitative phase microscopy of red blood cells during planar trapping and propulsion," Lab Chip **18**(19), 3025–3036 (2018).
55. K. Creath and G. Goldstein, "Dynamic quantitative phase imaging for biological objects using a pixelated phase mask," Biomed. Opt. Express **3**(11), 2866–2880 (2012).